Next-Generation Morphometry for pathomics-data mining in histopathology

Peter Boor (pboor@ukaachen.de)
RWTH Aachen University https://orcid.org/0000-0001-9921-4284

David Hölscher
RWTH Aachen University

Nassim Bouteldja
RWTH Aachen University

Mehdi Joodaki
RWTH Aachen University

Maria Russo
ondazione Ricerca Molinette, Torino

Yu-Chia Lan
RWTH Aachen University

Alireza Sadr
RWTH Aachen University

Mingbo Cheng
RWTH Aachen University

Vladimir Tesar
Charles University in Prague https://orcid.org/0000-0001-6982-0689

Saskia von Stillfried
RWTH Aachen University Hospital

Barbara Klinkhammer
RWTH Aachen University

Jonathan Barratt
John Walls Renal Unit, University Hospitals of Leicester, Leicester, UK

Juergen Floege
Universitätsklinikum Aachen

Ian Roberts
Oxford University Hospitals

Rosanna Coppo
Regina Margherita Hospital, Torino, Italy

Ivan Costa
RWTH Aachen University https://orcid.org/0000-0003-2890-8697

Roman Buelow

University Hospital RWTH Aachen https://orcid.org/0000-0002-8527-7353

Biological Sciences - Article

Keywords: Deep Learning, kidney biopsy, IgA Nephropathy, Computational Pathology

Posted Date: May 11th, 2022

DOI: https://doi.org/10.21203/rs.3.rs-1609168/v1

Next-Generation Morphometry for pathomics-data mining in histopathology

Running title: Automated segmentation and quantification of human kidney histopathology

David L. Hölscher[1,#], Nassim Bouteldja[1,#], Mehdi Joodaki[2], Maria L. Russo[3], Yu-Chia Lan[1], Alireza Vafaei Sadr[1], Mingbo Cheng[2], Vladimir Tesar[4], Saskia v. Stillfried[1], Barbara M. Klinkhammer[1], Jonathan Barratt[5,6], Jürgen Floege[7], Ian SD Roberts[8], Rosanna Coppo[3,9], Ivan G. Costa[2], Roman D. Bülow[1,§], Peter Boor[1,7,§,*]; for the International IgA Nephropathy Network[φ]

1 Institute of Pathology, RWTH Aachen University Clinic, Aachen, Germany
2 Institute for Computational Genomics, RWTH Aachen University Clinic, Aachen, Germany
3 Fondazione Ricerca Molinette, Torino, Italy
4 Department of Nephrology, 1st Faculty of Medicine and General University Hospital, Charles University, Prague, Czech Republic
5 John Walls Renal Unit, University Hospital of Leicester National Health Service Trust, Leicester, United Kingdom
6 Department of Cardiovascular Sciences, University of Leicester, Leicester, United Kingdom
7 Department of Nephrology and Immunology, RWTH Aachen University Clinic, Aachen, Germany
8 Department of Cellular Pathology, Oxford University Hospitals National Health Services Foundation Trust, Oxford, United Kingdom
9 Regina Margherita Children's University Hospital, Torino, Italy
φ Contributor information are provided at the end of the manuscript

Shared first authors
§ Shared senior authors

* Address correspondence to:
Peter Boor, M.D., Ph.D.
Institute of Pathology
RWTH Aachen University Hospital
Pauwelsstrasse 30
52074 Aachen, Germany
Phone: +49 241 80 85227
Fax: +49 241 80 82446
E-mail: pboor@ukaachen.de

Keywords: Deep Learning, kidney biopsy, IgA Nephropathy, Computational Pathology

Abstract

Pathology diagnostics relies on the assessment of morphological features by trained experts, which remains subjective and qualitative. Modern image analysis techniques, particularly deep learning, provide a possible solution, sometimes exceeding human capabilities, e.g., mutation prediction directly from histology. However, categorical model outputs are of limited use for further downstream analyses and limited interpretability. Here we developed a framework for large-scale histomorphometry (FLASH) which performs semantic segmentation and subsequent large-scale extraction of interpretable morphometric features. Two internal and three external, multi-centre cohorts of kidney biopsies were used to generate 40 million data points. Association with clinical data confirmed previous concepts, e.g., the importance of tubular atrophy for kidney function decline, and revealed unexpected findings, such as glomerular tuft hypertrophy in biopsies from patients with vs. without nephrotic range proteinuria. Single-structure analysis identified distinct glomerular populations and morphometric phenotypes along a trajectory of disease progression and features were independently associated with long-term clinical outcomes in IgA nephropathy. These data provide the concept for Next-generation Morphometry (NGM), opening new possibilities for comprehensive quantitative pathology data mining, i.e., pathomics, enabling augmented research and diagnostics.

Introduction

Pathology constitutes a cornerstone in the diagnosis and treatment decisions across many diseases. It mainly relies on morphology-based histopathological tissue analysis, which remains manual and requires highly trained expert pathologists. The same is true for nephropathology, a highly-specialised area of pathology focusing on the complex diagnostics of kidney diseases. Scoring systems applied by pathologists, such as the Banff-Classification[1] of kidney transplant pathology or the Oxford classification of IgA nephropathy (IgAN)[2], have improved standardisation in nephropathology. These scoring systems provide clinically important readouts, e.g., regarding response to therapy or assessing the likelihood of disease progression[1–3]. Despite such scoring systems, pathology diagnostics still remain semi-quantitative, labour-intensive, and subjective, sometimes with high inter-observer variability[4,5].

Progresses in digitisation of pathology enable workflows augmented by advanced image analysis techniques, particularly using deep learning (DL)[6,7]. End-to-end DL algorithms showed encouraging performances in various tasks, mainly explored in oncologic pathology, e.g., in tumour grading[8], subtyping of cancer variants[9] and prediction of mutation status[10]. These approaches, although promising, provide only qualitative or semi-

quantitative data and their explainability is limited, mostly remaining a "black-box"[11]. An approach to tackle these limitations and enable histopathology data mining is based on extraction of understandable quantitative features of histological structures[12–16]. This however requires precise and effective segmentation of relevant histopathological structures, which can be achieved using DL.

Here, we developed an automated framework for large scale histomorphometry (FLASH) in nephropathology. FLASH extends an existing DL-segmentation model[17] and is applicable to all morphological injury patterns across major kidney diseases. FLASH-derived quantitative morphometric features could be traced back directly to histology and reflected morphological alterations associated with disease progression, revealed novel associations of morphological alterations with clinical parameters, and provided independent prognostic factors for disease progression in IgAN.

Results

Demographic & clinical characteristics of cohort

Two internal, single-centre (*AC_B* & *AC_N*), and three external, multi-centre cohorts (*HubMAP, KPMP, VALIGA*) of kidney biopsies and nephrectomies were included (Figure 1A). Four cohorts (*AC_B, AC_N, HuBMAP, KPMP*) covering the whole spectrum of native and transplant pathology were used for development, testing and external validation of FLASH. The additional *VALIGA* cohort is a multicentric international cohort of IgAN patients, i.e., the most common glomerulonephritis worldwide, which was used to analyse the value of FLASH within a potential clinical setting. Demographic and clinical characteristics between cohorts were comparable, apart from younger patients and more males in the *VALIGA* cohort, as well as reduced kidney function assessed by estimated glomerular filtration rate (eGFR), which was more common in the *AC_B* cohort and a higher prevalence of hypertension in the *AC_N* cohort. Patient characteristics of all cohorts are provided in Supp. Table 1.

Precise pan-disease segmentation of kidney specimens

To enable quantitative data mining of kidney histology, the tissue must be precisely separated into relevant histopathological structures, such as glomeruli, tubules, vessels and interstitium. Two streamlined segmentation convolutional neural networks (CNNs) were trained to automate segmentation inference. One CNN was used for kidney tissue segmentation and another for instance-level (e.g., one glomerulus is one instance) structure segmentation of i) glomeruli, ii) their respective tufts, iii) tubules, iv) arteries, v) their respective lumina and vi) non-tissue background (annotation criteria are given in Supp. Table 2). Both segmentation CNNs showed high accuracies in the internal cohorts assessed by Dice-similarity-coefficients (on class- and instance-level), F1-score and positive predictive value (Table 1, Supp. Figure 1). The structure segmentation CNN correctly segmented glomeruli and glomerular tufts across all injury patterns, even in complex cases such as crescents, segmental sclerosis or a membranoproliferative pattern (Figure 2A). High accuracy was also observed for tubules despite large variations in size and shape, e.g., in tubular atrophy or light chain casts (Figure 3A). Arteries and especially their lumina were segmented with lower precision (Table 1). Regardless of large differences in staining protocols (Supp. Figure

2), segmentation accuracy was comparable or even better in the external, multi-centre cohorts used only for validation, indicating broad generalisability (Table 1, Supp. Figure 3). Small segmentation errors were detected in all classes (Supp. Figure 4).

Taken together, FLASH allowed a broad, "pan-disease" applicability across all common diseases and morphological injury patterns in multicentric kidney datasets.

Glomerular morphometry is associated with specific diseases and clinical readouts

Applying FLASH enabled the extraction of features of more than 11,000 glomeruli and glomerular tufts in the *AC_B* cohort, the subsequent large-scale comparisons of glomerular morphometric features (Supp. Table 3) and their distributions in common native kidney diseases (Figure 2C, Supp. Figure 5A-B). The median glomerular tuft area was significantly increased by 19.71% in lupus nephritis, 18.9% in minimal change disease (MCD) and 40.54% in membranous glomerulonephritis (GN) all with increased interquartile range (IQR) compared to the normal baseline (all $p < 0.01$, Figure 2C, Supp. Table 4). This effect could also be observed for full glomeruli (i.e., tuft + Bowman's space + capsule) in lupus nephritis (7.41% increase, $p < 0.01$), MCD (7.91% increase, $p < 0.01$) and membranous GN (25.21% increase, $p < 0.01$).

However, the change of the full glomerular area was less prominent than that of the tuft (Supp. Figure 5A, Supp. Table 4). In diabetic (DN) or hypertensive nephropathy (HTN) distributions of glomerular and tuft areas were more variable with larger IQRs. This was especially pronounced in HTN biopsies where the median glomerular tuft area was significantly increased while the percentage of glomeruli without a tuft (e.g., globally sclerotic or empty Bowman's space) was considerably higher as well (45.93% compared to 19.68%). This is likely due to glomerulosclerosis and hypertrophy of the remaining glomeruli.

Next, the hypothesis that proteinuria is associated with glomerular hypertrophy was investigated[18]. The glomerular tuft areas in native *AC_B* cases with vs. without nephrotic range proteinuria (i.e. > vs. <3.5g/d) were significantly larger (9.71%, $p < 0.01$, Figure 2D, Supp. Table 5). Analysis of diseases typically associated with proteinuria, i.e., MCD and membranous GN confirmed these findings with an average increase of mean tuft area by 10.69% in MCD and median tuft area by 51.01% in membranous GN (both $p < 0.01$, Figure 2D', Supp. Table 5). Interestingly, the median tuft area was slightly decreased in MCD suggesting that tuft hypertrophy only affects subgroups of glomeruli. A similar significant increase in glomerular tuft area by 18.7% was found in the *KPMP* cohort ($p < 0.01$, Figure 2D", Supp. Table 5). Tuft circularity in MCD was not significantly altered in nephrotic range proteinuria (0.41; IQR: 0.13 vs 0.40; IQR: 0.14, $p = 0.39$), suggesting that the

glomerular tufts were enlarged without changes in shape. In contrast, tuft circularity was significantly decreased by 19.57% ($p < 0.01$) in membranous GN with nephrotic range proteinuria, suggesting that the hypertrophic glomerular tufts in membranous glomerulonephritis were not solely upscaled, but also deformed (Figure 2E, Supp. Table 5).

In all native kidney biopsy cases from the *AC_B* cohort, the tuft circularity progressively decreased with kidney function loss (13.95% overall decrease, $p < 0.01$), in cases with eGFR >60 to eGFR of 30-60 (6.98% decrease, $p < 0.01$) to eGFR <30ml/min/1.73m^2 (7.5% decrease, $p < 0.01$, Figure 2F, Supp. Table 6). Furthermore, the tuft circularity was significantly reduced by 24.44% ($p < 0.01$) in DN and 18.89% ($p < 0.01$) in HTN compared to normal biopsies, associated with segmentally sclerotic tufts (Supp. Figure 5B, Supp. Table 4). However, the tuft circularity was significantly reduced by 20.0% ($p < 0.01$) in pauci-immune GN as well, likely reflecting the presence of crescents. This indicates that glomerular tuft deformation reflects structural alterations of glomeruli that are associated with deterioration of kidney function.

Taken together, FLASH allowed large scale quantitative analysis of glomerular morphometry, revealing novel clinico-morphological associations.

Morphometry of the tubulointerstitium and vasculature is linked to kidney function & hypertension

Since the tubulointerstitium and vasculature are often damaged in kidney diseases, FLASH was used to extract features of over two million tubular instances. These were compared based on the reported diagnosis, histopathological scoring and kidney function estimated by eGFR.

The tubular diameter significantly decreased in DN (by 16.04%), HTN (by 14.81%) and IgAN (by 4.58%) compared to normal biopsies (all $p < 0.01$, Supp. Figure 5C, Supp. Table 4). When grouping cases based on the interstitial fibrosis and tubular atrophy score (IFTA) taken from the pathology reports, the tubular diameters continuously decreased from none/marginal (0-10% IFTA) to mild (11-25% IFTA) to moderate (26-50% IFTA) to severe (>50% IFTA; all $p < 0.01$, Figure 3C, Supp. Table 7), reflecting an increase in tubular atrophy. Conversely, the tubular distance significantly increased in biopsies with mild (by 33.48%), moderate (by 44.12%) and severe IFTA (by 82.35%) compared to none/marginal IFTA (all $p < 0.01$, Figure 3D, Supp. Table 7), indicating an increase in interstitial space, which is most commonly due to interstitial fibrosis. Similar changes in the distribution of tubular morphometry were observed when cases were grouped based on stratified

eGFR. The tubular diameter progressively decreased with kidney function loss (5.84% overall decrease, $p < 0.01$), in cases with eGFR >60 to eGFR of 30-60 (2.63% decrease, $p < 0.01$) to eGFR <30ml/min/1.73m^2 (3.3% decrease, $p < 0.01$, Figure 3C', Supp. Table 6) while the tubular distance significantly increased (86.42% overall increase, $p < 0.01$) in cases with eGFR >60 to eGFR of 30-60 (39.81% increase, $p < 0.01$) to eGFR <30ml/min/1.73m^2 (33.33% increase, $p < 0.01$, Figure 3D', Supp. Table 6). Overall, the extracted tubulointerstitial features confirmed existing concepts of clinical and morphologic associations.

Arteriosclerosis is a common chronic vascular injury pattern in kidney diseases, currently only reported in gross grades. The artery wall diameter (i.e., wall thickness, Figure 3E) significantly increased in cases with none to moderate to severe reported arteriosclerosis (all $p < 0.01$), while the measured lumen diameters significantly decreased (all $p < 0.01$, Supp. Figure 6, Supp. Table 8). The median wall diameters of arteries and arterioles significantly increased by 8.59% ($p < 0.01$) in the *AC_B*, 10.85% ($p < 0.01$) in the *AC_N* and 20.33% ($p < 0.01$) in the *HuBMAP* cohort based on the presence of hypertension, likely due to thickening of the tunica media and intima (Figure 3F, Supp. Table 8). In the KPMP cohort an increase was also overserved (by 2.4%), although it was not significant ($p = 0.15$). As a result of increasing wall thickness, diameters of the arterial lumen decreased in all four cohorts (Supp. Table 8). Taken together, vascular features reflect the pathologist's

assessment of arteriosclerosis, are associated with the presence of hypertension and allow quantitative assessment of vascular alterations.

Morphometric features are predictive of disease progression in IgA nephropathy

To assess the utility of FLASH for outcome prediction in a clinical setting, the multicentric *VALIGA* cohort of IgAN patients was analysed. Disease progression was defined as reaching the combined endpoint of end-stage kidney disease (ESKD) and/or halving of the initial eGFR assessed at the time of biopsy within eight years after biopsy. Median follow-up time was 4.72 (IQR: 5.28) years. 14.29% of patients (n=92) reached the combined endpoint (16.31% due to ESKD, 23.91% due to eGFR halving and 59.78% due to both endpoints) within a median time of 4.53 (IQR: 5.17) years. Comparison of biopsies of patients reaching the combined endpoint vs. those who did not, revealed a significant decrease in tuft circularity (0.33; IQR: 0.08 vs. 0.38; IQR: 0.08, $p < 0.01$), tuft area (6,788.34; IQR: 3,628.64µm² vs. 9,296.31; IQR: 4,606.89µm², $p < 0.01$), tubular diameter (28.45; IQR: 7.09µm vs. 30.16; IQR: 6.53µm, $p < 0.01$), and a significant increase in tubular distance (4.57; IQR: 1.67µm vs 3.31; IQR: 1.85µm, $p < 0.01$), and Bowman's area (6,515.6; IQR: 1,630.71µm² vs. 6,009.81; IQR: 2,449.67µm², $p < 0.05$) (Figure 4A). Univariate Cox regression models for these five features showed that patients with

certain feature expressions at the time of biopsy displayed a faster decline of disease progression-free probability and a higher risk of reaching the combined endpoint (Figure 4B-C). Adjusted multivariate analysis for each predictive feature as well as age, sex, MEST-C score and eGFR at time of biopsy confirmed tubular distance (HR, 2.04; 95% CI 1.18-3.52, $p < 0.05$), tuft circularity (HR, 1.99; 95% CI 1.29-3.07, $p < 0.05$), tuft area (HR, 1.77; 95% CI 1.03-3.03, $p < 0.05$) and tubular diameter (HR, 1.82; 95% CI 1.13-2.92, $p < 0.05$) to be independent predictors for reaching the combined end-point, being significantly associated with disease progression (Supp. Table 9, Supp. Table 10). To further compare the digitally derived morphometric biomarkers with traditional histopathology scoring for IgAN, two Cox regression models were fitted, i) Digital Biomarkers (including all five digital features, age, sex and initial eGFR) and ii) *MEST-C* (including M, E, S, T, C, age, sex and initial eGFR) (Supp. Table 11). The fitted *Digital Biomarkers* model (C-statistic=0.80±0.03, AIC=1003, BIC=1023) was non-inferior to the *MEST-C* model (C-statistic=0.80±0.02, AIC=1010, BIC=1030). Combining the Digital Biomarkers and MEST-C model into a third, hybrid model resulted in a slight improvement (C-statistic=0.82±0.02, AIC=995, BIC=1028).

Glomerular morphometric phenotypes along disease progression trajectory

Animal models and experience from kidney biopsy diagnostics allow generating hypotheses on the course of morphological alterations during disease progression, however, an approach to quantitatively analyse this was missing. To tackle this, an unsupervised analysis using diffusion maps was performed to find major axes of glomerular morphometric changes in IgAN, revealing clusters of glomerular instances attributed to the overall kidney function measured by eGFR (Figure 5A-A"). Based on this, a trajectory and an estimated pseudotime score were determined, where glomeruli progress from a healthy to a diseased morphometric phenotype (Figure 5B). Histologic examples of glomeruli along the pseudotime supported morphological changes progressing from normal to increasingly diseased phenotypes with higher pseudotime scores, e.g., with increasing mesangial expansion and sclerosis (Figure 5B', Supp. Figure 7).

A feature expression heatmap along the pseudotime revealed glomerular morphometric alterations associated with IgAN disease progression, e.g., decreasing tuft area and tuft circularity, and increasing tuft eccentricity and elongation, resulting in smaller and more deformed glomerular tufts (Figure 5C). The fraction of glomerular instances at the beginning of the pseudotime

trajectory that belong to patients with preserved kidney function (>60ml/min/1.73m^2) continuously decreased along the pseudotime (Figure 5D). On the other hand, the fraction of glomeruli from patients with considerably reduced kidney function (<30ml/min/1.73m^2) constantly increased along the pseudotime trajectory, indicating that the pseudotime represents the disease progression of IgAN towards ESKD in glomerular populations (Figure 5D).

Automated visualisation of image patches enabled displaying morphometric outliers of glomeruli and in a single, representative case of IgAN from the *AC_B* cohort. Morphometric outliers of structures of interest were displaying various pathological lesions i.e., crescents, segmental sclerosis or tubular atrophy (Supp. Figure 8) which could enable fast-track assessment of kidney histopathology.

Discussion

Our study presents a proof-of-concept for large-scale automated extraction of large-scale quantitative morphometric data from histopathology, i.e., Next-Generation Morphometry (NGM). For this, a DL-based instance segmentation and quantification framework (FLASH) was implemented. FLASH was developed and validated in heterogeneous multi-centre datasets using both kidney biopsies and nephrectomies and a large variety of diseases. The segmentation accuracy of FLASH was high across cohorts, indicating broad generalisability. We focused on nephropathology, since the kidney is one of the most complex organs in pathology diagnostics, requiring a high level of specialisation, and representing a challenging use case. NGM provides the basis for histopathology morphometry, a novel "omics" approach we propose to term "pathomics".

Omics technologies comprehensively quantify biomolecules in an unbiased manner and on a large scale, e.g., DNA in genomics, RNA in transcriptomics and proteins in proteomics[19]. These approaches are increasingly performed in a comprehensive, multi-omics fashion[20] and with spatial resolution[21,22]. Although morphological alterations in diseases are very well recognized and have been used for diagnostics for over a century, approaches for omics-based analysis of histopathology were missing. NGM and pathomics could serve as a novel, complementary approach to the molecular omics

techniques, providing unbiased, tissue-based, quantitative (geometrical) information on histological structures. Compared to established omics techniques, which are continuously improved, NGM is currently in its infancy. It is expected that NGM will undergo prominent development, particularly given that the technological prerequisites are largely met, i.e., the instruments for high-throughput digitisation of histology slides, graphics processing units (GPUs) and storage are increasingly being available and affordable. E.g., in this study we were able to analyse 7,382,198 instances of histological structures with 6,742,314 tubules, 89,160 glomeruli and 550,724 arteries, showing that NGM can be used to provide data on histology at an unprecedented scale.

Similarly to Next-generation Sequencing and genomics, which have revolutionised research and diagnostics by comprehensive genetic molecular characterisation, NGM opens new frontiers in quantitative assessment of morphology. As a first proof-of-concept we have shown the potential utility of NGM and pathomics for quantitative kidney histopathology data mining, providing clinically relevant and complementary readouts that can constitute an important step towards precision medicine.

Patients with MCD or membranous GN and nephrotic range proteinuria showed a prominent increase in mean glomerular tuft area, compared to those without. In MCD-patients, larger glomeruli identified by manual analysis were previously associated with an increased risk for kidney function

deterioration and development of glomerular sclerosis[23]. With FLASH and NGM, such morphological biomarkers can now be assessed automatically across all diseases. Importantly, FLASH revealed a decrease in tuft circularity in membranous GN patients with nephrotic range proteinuria, but not in MCD, indicating different mechanisms of glomerular hypertrophy in these diseases. The tuft circularity progressively decreased across all native diseases in patients with decreased kidney function, indicating that this might be a general feature of kidney function decline. Thereby, NGM can provide novel findings and generate novel research questions based on morphology.

NGM and FLASH enabled the identification of morphological features that are independent predictors of kidney function decline in IgAN, such as the smallest distance between tubular instances, the glomerular tuft circularity or the tubular diameter. While some of these were expected, e.g., the distance between tubules reflecting interstitial fibrosis, others, such as tuft circularity, were unexpected. These features could be used as a set of digital biomarkers, potentially improving the predictive value and reproducibility of histopathology diagnostics. Accordingly, a combined model of only a few of these digital biomarkers proved to be non-inferior compared to a validated standard histopathological scoring system, i.e., the MEST-C score[24]. The advantage of using NGM over a pathologist-derived score is that it is quantitative and fully automated, thereby better reproducible, more precise and faster, sparing the time of pathologists.

Adapting techniques designed to analyse other omics data, such as single cell sequencing data, we identified a trajectory of disease progression in a low dimensional embedding of glomerular features in IgAN. This allowed a granular analysis of progression of glomerular phenotypes from healthy to diseased, which can be seen as a novel and unbiased way of identifying histologic features relevant for disease progression. This first proof of concept shows that NGM-based data can be used to make histopathology analysis quantitative, capturing more subtle changes which better reflect the biological reality of disease progression and modelling disease progression relevant pathologies.

Some studies previously described the potential of morphometric analysis of histology[17,25–28]. Although very specific, these scoring systems were applicable only in specific use cases and particular pathological alterations. NGM and FLASH follow a holistic approach of morphometric analysis, prioritising unbiased data mining, thus enabling a wider variety of possible downstream analyses, i.e., an exploratory approach comparable to other omics techniques.

Currently, a major focus in computational pathology is the development of end-to-end DL solutions, which mostly provide qualitative results, e.g., a disease class or mutational status[10,29–31]. On the contrary, NGM and FLASH use segmentation as a basis for subsequent large-scale quantitative data mining. Compared to end-to-end pipelines, NGM provides an alternative

approach with several advantages. The results are visually verifiable, can be easily checked by pathologists, and are therefore interpretable. This is often not the case in end-to-end DL solutions, which remain a black-box in terms of explainability. Therefore, quantitative histology features remain comprehensible, even if clustered in a lower dimensional space. This can help reduce potential scepticism towards DL based systems that might hinder clinical application.

In nephropathology, the majority of cases, including IgAN, are rare diseases. Large data repositories allowing the effective and robust development of end-to-end DL pipelines in nephropathology are missing, making the development of such pipelines considerably more difficult compared to oncological pathology. In comparison, NGM and FLASH do not require large datasets for development and can be applied to any type of disease, including rare diseases such as in MCD, IgAN, etc.

This study has several important limitations. Currently, FLASH includes only a few, easily explainable morphometric features, focusing on providing a proof-of-concept of the utility of NGM. One of the challenges we encountered was the large variability within the stainings, which prohibited us from extracting additional features, e.g., colour or texture-based features. Further developments should focus on colour normalisation approaches, a larger number of additional morphological features, and inclusion of subvisual features to provide even more comprehensive morphometric data.

Another limitation is that FLASH is not generic for any kind of tissue, but specifically developed for the kidney. Particularly because of the required tissue-specific segmentation and different stains used in various organ histopathology analysis, it is currently unlikely to have a pipeline applicable for every kind of tissue histology. In addition, generating the ground truth for the segmentation algorithm requires considerable effort and time-investment by expert pathologists, which is a limitation in comparison to end-to-end approaches, which can be trained in a weakly supervised way with very little manual overhead. Another limitation is the retrospective design of this study. However, this study should serve as the basis for designing potential future prospective trials investigating the predictive potential of NGM.

In conclusion, our study lays the groundwork for introducing NGM and pathomics for explainable, quantitative, histopathology analysis and pathomics.

Methods

Cohort assembly & sample collection

For development, validation and application of FLASH, whole-slide images (WSIs) and clinical data from five cohorts were gathered (Supp. Table 12): two

internal (development cohorts) and three external, two of which were used for validation and the third, the *VALIGA* trial, for a disease-specific application use case (Figure 1A). Following exclusion criteria were used in all cohorts: i) no kidney tissue in the specimen, ii) no Periodic Acid Schiff (PAS)-slide available, iii) only cryosections available and iv) containing less than eight glomeruli, unless a definitive pathological diagnosis could be made, v) large artefacts present on the slide, vi) insufficient scan quality (e.g., major part of tissue being out of focus and blurred), vii) insufficient stain quality (e.g., unstained tissue) and viii) broken slides (Figure 1A).

Data collection and analysis in this study was approved by the local ethic committee of the RWTH Aachen University (EK-No. 315/19).

Development cohorts

Aachen Biopsy cohort (*AC_B*). A database search identified 355 kidney biopsy cases in the archive of the Institute of Pathology of the RWTH Aachen university clinic within the inclusion period (January 1st 2017 - May 1st 2021). Biopsies were either native kidney or indication or protocol transplant biopsies. Diagnoses for all cases are given in Supp. Table 13.

Aachen Nephrectomy cohort (*AC_N*). 38 nephrectomy specimens (inclusion period: 2013 - 2021) were included, appreciating that nephropathology is not limited to biopsy specimens and aiming at applicability also in nephrectomy samples. The *AC_N* cohort consists of 13 transplant nephrectomies due to

severe complications and 25 tumour nephrectomies, including only non-tumour tissue away from tumour borders. Both groups reflect a broad morphological spectrum of histopathology. More tumour nephrectomies than transplant nephrectomies were included since they are more common in routine diagnostics.

In both cohorts 1-3 µm thick formalin-fixed and paraffin-embedded (FFPE) sections were used. All slides from the *AC_B*, *AC_N* and *VALIGA* cohorts were digitised using an Aperio AT2 whole-slide scanner with a 40x objective (Leica Biosystems, Wetzlar, Germany).

External validation cohorts

Two external publicly available cohorts from independent consortia were included to validate the generalisability of our CNNs. The cohort from the Kidney Precision Medicine Project (KPMP)[32] (accessed on 15th March 2021) consists of 90 PAS-stained WSIs from patients with either acute kidney injury (AKI), chronic kidney disease (CKD) or healthy tumour nephrectomies. It included 34 biopsy and two nephrectomy cases. After the exclusion process, 85 PAS-stained WSIs were included in the analysis. The cohort from the Human BioMolecular Atlas Program (HubMAP)[33] contains 22 nephrectomy specimens from 12 deceased organ donors. 13 cryo sections were excluded since they were out of distribution (we only trained on FFPE material), with the final cohort consisting of nine nephrectomy WSIs from nine cases.

Additionally, clinical data from both cohorts were gathered when available (Supp. Table 12).

Specific application cohort

After development was finished, the FLASH architecture was applied to the multi-centre *VALIGA* trial which represents one of the largest biopsy cohorts of patients with IgAN. From the initial cohort, 768 cases could be identified and digitised (scanned). The following problems prevented more cases from being included: a) it was not possible to identify the slide label (e.g., because it faded, or fell off), or b) slides broke during transport. Overall, 106 cases were excluded, since they met at least one of the above-mentioned exclusion criteria, most often not available digital PAS-stained slides. An additional 14 cases were excluded on slide level due to artefacts, with in total, 648 PAS-stained WSIs of 648 cases being included (Figure 1A).

Framework development

FLASH consists of an automated three-step approach: i) a CNN that automatically segments kidney tissue on a WSI discarding all non-kidney tissues (e.g., adipose or muscle tissue), ii) another CNN that segments histological structures of the kidney tissue segmented by the first CNN and iii) hand-crafted feature extraction for segmented structures (Figure 1B). The

framework is applicable to the whole morphological spectrum of non-neoplastic kidney diseases.

Generation of annotations

For the kidney tissue segmentation, we annotated kidney tissue on slide-level. For the segmentation of histological structures, we annotated patches of size 174x174µm² using the following six classes (Supp. Table 2): (1) full glomerulus (including the tuft), (2) glomerular tuft, (3) tubule, (4) artery (including lumen, intima and media), (5) arterial lumen and (6) non-tissue background (including veins with a diameter of >30µm). We focused on these classes since they represent the major kidney compartments and can be reproducibly annotated even in severe diseases. Further details on the annotation process are described in the supplementary methods. Overall, we annotated 1,056 WSIs for the tissue segmentation and 4,031 patches and 27,287 structures for the structure segmentation in the four development and validation cohorts (Supp. Tables 14-15). Two medical students and two nephropathologists were involved in the annotation process.

Tissue & structure segmentation CNNs

For the segmentation of kidney tissue, we used an nnU-Net, representing the state-of-the-art for biomedical image segmentation[34]. For the segmentation

of histological structures, we have built on our previous study on kidney structure segmentation in experimental nephropathology by employing the same U-Net-like architecture and training routine as they were specifically developed and comprehensively validated for this particular task[17]. Both CNNs were developed using the internal *AC_B* and *AC_N* cohorts while the external held-out data from the *KPMP* and *HuBMAP* cohorts were used for external validation only. Detailed information on CNN architecture and training routines including data splits is provided in the supplementary methods.

Performance evaluation

Segmentation accuracy was assessed by Dice-similarity-coefficients (DSC) for the tissue segmentation. Instance Dice-similarity-coefficients (iDSC) were used for the structure segmentation, in which the differentiation of individual instances is essential. In addition to DSCs and iDSCs, other established metrics such as F1-Scores and positive predictive values (PPVs) were assessed. Performance metrics were calculated by averaging scores for all prediction and ground truth instances from all slides of the test/validation set.

Feature extraction

FLASH enabled us to extract 7,382,198 instances of segmented histological structures (6,742,314 tubules, 89,160 glomeruli and 550,724 arteries) from the five cohorts. Each segmented instance represents a geometrical object, enabling the quantitative assessment of 35 hand-crafted morphometric histological features including area, shape, diameter or distance. Due to very large divergence in staining in the multicentric cohorts, the extraction of colour or texture-based features was not feasible. Additional information regarding the computation of morphometrical features is given in the supplementary methods and in Supp. Table 3.

Single structure trajectory analysis

We used Seurat (4.1.0 version)[35] to perform a single structure trajectory analysis. We considered structures as samples and structure features as columns. This analysis was done independently for tubules and glomeruli due to distinct features. Next, we ran NormalizeData with the parameter normalization.method='RC' (Relative counts) to normalise each structure. We used the Corral package (version 1.4.0)[36] to perform dimension reduction using Pearson Residuals based correspondence analysis. Next, we produced a diffusion map using the destiny package (3.8.1)[37] with default parameters. We performed Louvain clustering with the first two components of diffusion

embeddings by calling FindNeighbors and FindClusters from the Seurat package. Finally, we found trajectories using ArchR (version 1.0.1)[38]. Specifically, we first defined a backbone by selecting a list of clusters from healthy to disease and using their function addTrajectory to detect a pseudo-time scale from 0 to 100. For line plots, we distributed all patients to 20 buckets from 0 to 100 and calculated the fractions in each bucket of each condition. We next fitted smoothed lines using method loess (locally estimated scatterplot smoothing).

Statistical analyses

All statistical calculations were performed within the computing environment R (v4.0.3). We performed two-sample k-sample Anderson-Darling tests[39] for comparison between different feature distributions. Comparing groups with smaller sample sizes, e.g., specimen-level comparison of histopathology, we performed a Kruskal-Wallis test and two-sided pairwise Wilcoxon rank-sum tests. For multiple comparisons, e.g., diseases, we corrected for multiple testing by Bonferroni-type adjustment. Probabilities of progression-free survival for *VALIGA* biopsies were assessed by calculating Cox regression models with hazard ratios (HR) and 95% confidence intervals. Categorical variables were interpreted as absolute (n) and relative (%) frequencies while descriptive continuous features were

described as mean/median + IQR. Values of $p < 0.05$ were considered significant.

Code and data availability

Whole-slide images from our internal cohorts and the *VALIGA* trial cannot be made publicly available due to regulatory reasons. All data from the external cohorts are publicly available (at atlas.kpmp.org/repository & portal.hubmapconsortium.org). NGM data and the trained FLASH models will be made available to interested research partners on reasonable request to the corresponding author. The source code of FLASH is freely accessible including user instructions at: git-ce.rwth-aachen.de/labooratory-ai/flash.

Author contributions

DLH, RDB and PB conceived and designed the study. DLH, MLR, VT, SvS, BMK, JB, JF, IR, RC and RDB collected and digitised patient cohorts or provided clinical data. DLH, MLR, VT, JB, JF, IR, RC and RDB assigned

patients to classes. DLH, RDB and PB performed annotations and quality controls. NB and YL performed deep learning analyses and visualisations. DLH, NB, MJ, AVS, MC, IGG and RDB performed data analysis. DLH wrote the initial draft of the manuscript. DLH and RDB created the figures. All authors subsequently read and revised the manuscript and read and approved the final version. All authors had access to all the data in the study and DLH, NB, RDB and PB verified the data and had final responsibility for the decision to submit for publication.

Group information

The International IgA Nephropathy Network members are as follows:
VALIGA investigators: M.L. Russo (MA, PhD, Fondazione Ricerca Molinette, Torino, Italy); S. Troyanov (MD, Division of Nephrology, Department of Medicine, Hopital du Sacre-Coeur de Montreal, Montreal, Quebec, Canada); H.T. Cook (MD, Centre for Complement and Inflammation Research, Department of Medicine, Imperial College, London, England); I. Roberts (MD, Department of Cellular Pathology, Oxford University Hospitals NHS Foundation Trust, John Radcliffe Hospital, Oxford, United Kingdom); V. Tesar, (MD, Department of Nephrology, 1st Faculty of Medicine and General University Hospital, Charles University, Prague, Czech Republic); D. Maixnerova (MD, Department of Nephrology, 1st Faculty of Medicine and General University Hospital, Charles University, Prague, Czech Republic); S. Lundberg (MD, Nephrology Unit, Department of Clinical Sciences, Karolinska Institute, Stockholm, Sweden); L. Gesualdo (MD, Department of Nephrology, Emergency and Organ Transplantation, University of Bari "Aldo Moro," Foggia-Bari, Italy); F. Emma (MD, Division of Nephrology, Department of Pediatric Subspecialties, Bambino Gesù Children's Hospital IRCCS, Rome, Italy); F. Diomedi (MD, Division of Nephrology, Department of Pediatric Subspecialties, Bambino Gesù Children's Hospital IRCCS, Rome, Italy); G. Beltrame (MD, Nephrology and Dialysis Unit, San Giovanni Bosco Hospital, and University of Turin,Turin, Italy); C. Rollino (MD, Nephrology and Dialysis Unit, San Giovanni Bosco Hospital, and University of Turin,Turin, Italy); A. Amore (MD, Nephrology Unit, Regina

Margherita Children's Hospital,Turin, Italy); R. Camilla (MD Nephrology Unit, Regina Margherita Children's Hospital, Turin, Italy); L. Peruzzi (MD, Nephrology Unit, Regina Margherita Children's Hospital, Turin, Italy); M. Praga (MD, Nephrology Unit, Hospital 12 de Octubre,Madrid, Spain); S. Feriozzi (MD, Nephrology Unit, Belcolle Hospital, Viterbo, Italy), R. Polci, (MD, Nephrology Unit, Belcolle Hospital,Viterbo, Italy); G. Segoloni, (MD, Division of Nephrology Dialysis and Transplantation, Department of Medical Sciences, Città della Salute e della Scienza Hospital and University of Turin, Turin, Italy); L.Colla (MD, Division of Nephrology Dialysis and Transplantation, Department of Medical Sciences, Città della Salute e della Scienza Hospital and University of Turin,Turin, Italy); A. Pani (MD, Nephrology Unit, G. Brotzu Hospital, Cagliari, Italy); D. Piras (MD, Nephrology Unit, G. Brotzu Hospital, Cagliari, Italy), A. Angioi (MD, Nephrology Unit, G. Brotzu Hospital, Cagliari, Italy); G. Cancarini, (MD, Nephrology Unit, Spedali Civili University Hospital, Brescia, Italy); S. Ravera (MD, Nephrology Unit, Spedali Civili University Hospital, Brescia, Italy); M. Durlik (MD, Department of Transplantation Medicine, Nephrology, and Internal Medicine, Medical University ofWarsaw,Warsaw, Poland); E. Moggia (Nephrology Unit, Santa Croce Hospital, Cuneo, Italy); J. Ballarin (MD, Department of Nephrology, Fundacion Puigvert, Barcelona, Spain); S. Di Giulio (MD, Nephrology Unit, San Camillo Forlanini Hospital, Rome, Italy); F. Pugliese (MD, Department of Nephrology, Policlinico Umberto I University Hospital, Rome, Italy); I. Serriello (MD, Department of Nephrology, Policlinico Umberto I University Hospital, Rome, Italy); Y. Caliskan (MD, Division of Nephrology, Department of Internal Medicine, Istanbul Faculty of Medicine, Istanbul University, Istanbul, Turkey); M. Sever (MD, Division of Nephrology, Department of Internal Medicine, Istanbul Faculty of Medicine, Istanbul University, Istanbul, Turkey); I. Kilicaslan (MD, Department of Pathology, Istanbul Faculty of Medicine, Istanbul University, Istanbul, Turkey); F. Locatelli (MD, Department of Nephrology and Dialysis, Alessandro Manzoni Hospital, ASST Lecco, Italy); L. Del Vecchio (MD, Department of Nephrology and Dialysis, Alessandro Manzoni Hospital, ASST Lecco, Italy); J.F.M.Wetzels (MD, Departments of Nephrology, Radboud University Medical Center, Nijmegen, the Netherlands); H. Peters (MD, Departments of Nephrology, Radboud University Medical Center, Nijmegen, the Netherlands); U. Berg (MD, Division of Pediatrics, Department of Clinical Science, Intervention and Technology, Huddinge, Sweden); F. Carvalho (MD, Nephrology Unit, Hospital de Curry Cabral, Lisbon, Portugal); A.C. da Costa Ferreira (MD, Nephrology Unit, Hospital de Curry Cabral, Lisbon, Portugal); M. Maggio (MD, Nephrology Unit, Hospital Maggiore di Lodi, Lodi, Italy); A. Wiecek (MD, Department Nephrology, Endocrinology and Metabolic Diseases, Silesian University of Medicine, Katowice, Poland); M. Ots-Rosenberg(MD, Nephrology Unit, Tartu University Clinics, Tartu,Estonia); R. Magistroni (MD, Department of Nephrology, Policlinic of Modena and Reggio Emilia; Modena, Italy); R. Topaloglu

(MD, Department of Pediatric Nephrology and Rheumatology, Hacettepe University, Ankara, Turkey); Y. Bilginer (MD, Department of Pediatric Nephrology and Rheumatology, Hacettepe University, Ankara, Turkey); M. D'Amico (MD, Nephrology Unit, S. Anna Hospital, Como, Italy); M. Stangou (MD, Department of Nephrology, Hippokration General Hospital, Aristotle University of Thessaloniki, Thessaloniki, Greece); F. Giacchino (MD, Nephrology Unit, Ivrea Hospital, Ivrea, Italy); D. Goumenos (MD Department of Nephrology, University Hospital of Patras, Patras, Greece); P. Kalliakmani (MD Department of Nephrology, University Hospital of Patras, Patras, Greece); M. Papasotiriou (MD Department of Nephrology, University Hospital of Patras, Patras, Greece); K. Galesic (MD, Department of Nephrology, University Hospital Dubrava, Zagreb, Croatia); C. Geddes (MD, Renal Unit,Western Infirmary Glasgow, Glasgow, United Kingdom); K. Siamopoulos (MD, Nephrology Unit, Medical School University of Ioanina, Ioannina, Greece); O. Balafa (MD, Nephrology Unit,Medical School University of Ioanina, Ioannina, Greece); M. Galliani (MD, Nephrology Unit, S.Pertini Hospital, Rome, Italy); P. Stratta (MD, Department of Nephrology, Maggiore della Carità Hospital, Piemonte Orientale University, Novara, Italy); M. Quaglia (MD, Department of Nephrology, Maggiore della Carità Hospital, Piemonte Orientale University, Novara, Italy); R. Bergia (MD, Nephrology Unit, Degli Infermi Hospital, Biella,Italy); R. Cravero (MD, Nephrology Unit, Degli Infermi Hospital, Biella, Italy); M. Salvadori, (MD, Department of Nephrology, Careggi Hospital, Florence, Italy); L. Cirami (MD, Department of Nephrology, Careggi Hospital, Florence, Italy); B. Fellstrom (MD, Renal Department, University of Uppsala, Uppsala, Sweden); H. Kloster Smerud (MD, Renal Department, University of Uppsala, Uppsala, Sweden); F. Ferrario (MD, Nephropathology Unit, San Gerardo Hospital, Monza, Italy); T. Stellato (MD, Nephropathology Unit, San Gerardo Hospital, Monza, Italy); J. Egido (MD, Department of Nephrology, Fundacion Jimenez Diaz, Madrid, Spain); C. Martin (MD, Department of Nephrology, Fundacion Jimenez Diaz, Madrid, Spain); J. Floege (MD, Nephrology and Immunology, Medizinische Klinik II, University of Aachen, Aachen, Germany); F. Eitner (MD, Nephrology and Immunology, Medizinische Klinik II, University of Aachen, Aachen, Germany); A. Lupo (MD, Department of Nephrology, University of Verona, Verona, Italy); P. Bernich (MD, Department of Nephrology, University of Verona, Verona, Italy); P. Menè (Department of Nephrology,S. Andrea Hospital, Rome, Italy); M. Morosetti (Nephrology Unit, Grassi Hospital, Ostia, Italy); C. van Kooten, (MD, Department of Nephrology, Leiden University Medical Centre, Leiden, The Netherlands); T. Rabelink (MD, Department of Nephrology, Leiden University Medical Centre, Leiden, The Netherlands); M.E.J. Reinders (MD, Department of Nephrology, Leiden University Medical Centre, Leiden, The Netherlands); J.M. Boria Grinyo (Department of Nephrology, Hospital Bellvitge, Barcelona, Spain); S. Cusinato (MD, Nephrology Unit, Borgomanero Hospital, Borgomanero, Italy); L. Benozzi (MD, Nephrology Unit, Borgomanero

Hospital, Borgomanero, Italy); S. Savoldi, (MD, Nephrology Unit, Civile Hospital, Ciriè, Italy); C. Licata (MD, Nephrology Unit, Civile Hospital, Ciriè, Italy); M. Mizerska-Wasiak (MD, Department of Pediatrics, Medical University ofWarsaw,Warsaw, Poland); G. Martina (MD, Nephrology Unit, Chivasso Hospital, Chivasso, Italy); A. Messuerotti (MD, Nephrology Unit, Chivasso Hospital, Chivasso, Italy); A. Dal Canton (MD, Nephrology Unit, S. Matteo Hospital, Pavia, Italy); C. Esposito (MD, Nephrology Unit, Maugeri Foundation, Pavia, Italy); C. Migotto (MD, Nephrology Unit, Maugeri Foundation, Pavia, Italy); G. Triolo MD, Nephrology Unit CTO, Turin, Italy); F.Mariano (MD, Nephrology Unit CTO, Turin, Italy); C. Pozzi (MD, Nephrology Unit, Bassini Hospital, Cinisello Balsamo, Italy); R. Boero (MD, Nephrology Unit, Martini Hospital, Turin, Italy);

VALIGA pathology investigators: S. Bellur (MD, Department of Cellular Pathology, Oxford University Hospitals NHS Foundation Trust, John Radcliffe Hospital, Oxford, United Kingdom); G.Mazzucco (MD, Pathology Department, University of Turin, Turin, Italy); C. Giannakakis (MD, Pathology Department, La Sapienza University, Rome, Italy); E. Honsova (MD, Department of Clinical and Transplant Pathology, Institute for Clinical and Experimental Medicine, Prague, Czech Republic); B. Sundelin (MD Department of Pathology and Cytology, Karolinska University Hospital, Karolinska Institute, Stockholm, Sweden); A.M. Di Palma (Nephrology Unit, Aldo Moro University, Foggia-Bari, Italy); F. Ferrario (MD, Nephropathology Unit, San Gerardo Hospital, Monza, Italy); E. Gutiérrez (MD, Renal, Vascular and Diabetes Research Laboratory, Fundación Instituto de Investigaciones Sanitarias-Fundación Jiménez Díaz, Universidad Autónoma de Madrid, Madrid, Spain); A.M. Asunis (MD, Department of Pathology, Brotzu Hospital, Cagliari, Italy); J. Barratt (MD, The JohnWalls Renal Unit, Leicester General Hospital, Leicester, United Kingdom); R. Tardanico (MD, Department of Pathology, Spedali Civili Hospital, University of Brescia, Brescia, Italy); A. Perkowska-Ptasinska (MD, Department of Transplantation Medicine, Nephrology and Internal Medicine, Medical University of Warsaw, Warsaw, Poland); J. Arce Terroba (MD, Pathology Department, Fundació Puigvert, Barcelona, Spain); M. Fortunato (MD, Pathology Department, S. Croce Hospital, Cuneo, Italy); A. Pantzaki (MD, Department of Pathology, Hippokration Hospital, Thessaloniki, Greece); Y. Ozluk (MD, Department of Pathology, Istanbul University, Istanbul Faculty of Medicine, Istanbul, Turkey); E. Steenbergen (MD, Radboud University Medical Center, Department of Pathology, Nijmegen, The Netherlands); M. Soderberg (MD, Department of Pathology, Drug Safety and Metabolism, Huddinge, Sweden); Z. Riispere (MD, Department of Pathology, University of Tartu, Tartu, Estonia); L. Furci (MD, Pathology Department, University of Modena, Italy); D. Orhan (MD, Department of Pediatrics, Division of Rheumatology, Hacettepe University Faculty of Medicine, Ankara, Turkey); D. Kipgen (MD,Pathology Department, Queen Elizabeth University Hospital, Glasgow, United Kingdom); D. Casartelli (Pathology

Department, Manzoni Hospital, Lecco, Italy); D. Galesic Ljubanovic (MD, Nephrology Department, University Hospital, Zagreb, Croatia; Zagreb, Croatia); H Gakiopoulou (MD, Department of Pathology, National and Kapodistrian University of Athens, Athens, Greece); E. Bertoni (MD, Nephrology Department, Careggi Hospital, Florence, Italy); P. Cannata Ortiz (MD, Pathology Department, IIS-Fundacion Jimenez Diaz UAM, Madrid, Spain); H. KarkoszkaMD, (Nephrology, Endocrinology and Metabolic Diseases, Medical University of Silesia, Katowice, Katowice, Poland); H.J. Groene (MD, Cellular and Molecular Pathology, German Cancer Research Center, Heidelberg, Germany); A. Stoppacciaro (MD, Surgical Pathology Units, Department of Clinical and Molecular Medicine, Ospedale Sant'Andrea, Sapienza University of Rome, Rome, Italy); I. Bajema (MD, Department of Pathology, Leiden University Medical Center, Leiden, The Netherlands); J. Bruijn (MD, Department of Pathology, Leiden University Medical Center, Leiden, The Netherlands); X. Fulladosa Oliveras (MD, Nephrology Unit, Bellvitge University Hospital, Hospitalet de Llobregat, Barcelona, Spain); J. Maldyk (MD, Division of Pathomorphology, Children's Clinical Hospital, Medical University ofWarsaw,Warsaw, Poland); and E. Ioachim (MD, Department of Pathology, Medical School, University of Ioannina, Ioannina, Greece); the Oxford derivation and North American validation investigators: Bavbek N (MD, Department of Pathology, Vanderbilt University, Nashville, Tennessee); Cook T (MD, Imperial College, London, England), Troyanov S (MD, Division of Nephrology, Department of Medicine, Hopital du Sacre-Coeur de Montreal, Montreal, Quebec, Canada); Alpers C (MD, Department of Pathology, University of Washington Medical Center, Seattle,Washington), Amore A (MD, Nephrology, Dialysis and Transplantation Unit, Regina Margherita Children's Hospital, University of Turin, Turin, Italy), Barratt J (MD, The John Walls Renal Unit, Leicester General Hospital, Leicester, England); Berthoux F (MD, Department of Nephrology, Dialysis, and Renal Transplantation, Hôpital Nord, CHU de Saint-Etienne, Saint-Etienne, France); Bonsib S (MD, Department of Pathology, LSU Health Sciences Center, Shreveport, Los Angeles); Bruijn J (MD, Department of Pathology, Leiden University Medical Center, Leiden, The Netherlands); D'Agati V (MD, Department of Pathology, Columbia University College of Physicians & Surgeons, New York, New York); D'Amico G (MD, Fondazione D'Amico per la Ricerca sulle Malattie Renali, Milan, Italy); Emancipator S (MD, Department of Pathology, Case Western Reserve University, Cleveland, Ohio); Emmal F (MD, Division of Nephrology and Dialysis, Department of Nephrology and Urology, Bambino Gesù Children's Hospital and Research Institute, Piazza S Onofrio, Rome, Italy); Ferrario F (MD, Renal Immunopathology Center, San Carlo Borromeo Hospital, Milan, Italy); Fervenza F (MD PhD, Division of Nephrology and Hypertension, Mayo Clinic, Rochester); Florquin S (MD, Department of Pathology, Academic Medical Center, University of Amsterdam, Amsterdam, The

Netherlands); Fogo A (MD, Department of Pathology, Vanderbilt University, Nashville, Tennessee); Geddes C (MD, The Renal Unit, Western Infirmary, Glasgow, Scotland); Groene H (MD, Department of Cellular and Molecular Pathology, German Cancer Research Center, Heidelberg, Germany); Haas M(MD, Department of Pathology and Laboratory Medicine, Cedars-Sinai Medical Center, Los Angeles, California); Hill P (MD, St Vincent's Hospital, Melbourne, Australia); Hogg R (MD, Scott and White Medical Center, Temple, Texas (retired)); Hsu S (MD, Division of Nephrology, Hypertension and Renal Transplantation, College of Medicine, University of Florida, Gainesville, Florida); Hunley T (MD, Department of Pathology, Vanderbilt University, Nashville, Tennessee); Hladunewich (MD, Division of Nephrology, Sunnybrook Health Science Center, University of Toronto, Ontario, Canada M); Jennette C (MD, Department of Pathology and Laboratory Medicine, University of North Carolina, Chapel Hill, North Carolina); Joh K (MD, Division of Immunopathology, Clinical Research Center Chiba, East National Hospital, Chiba, Japan); Julian B (MD, Department of Medicine, University of Alabama at Birmingham, Birmingham, Alabama); Kawamura T (MD, Division of Nephrology and Hypertension, Jikei University School of Medicine, Tokyo, Japan); Lai F (MD, The Chinese University of Hong Kong, Hong Kong); Leung C (MD, Department of Medicine, Prince of Wales Hospital, Chinese University of Hong Kong, Hong Kong); Li L (MD, Research Institute of Nephrology, Jinling Hospital, Nanjing University School of Medicine, Nanjing, China); Li P (MD, Department of Medicine, Prince of Wales Hospital, Chinese University of Hong Kong, Hong Kong); Liu Z (MD, Research Institute of Nephrology, Jinling Hospital, Nanjing University School of Medicine, Nanjing, China); Massat A (MD, Division of Nephrology and Hypertension, Mayo Clinic, Rochester, Minnesota); Mackinnon B (MD, The Renal Unit,Western Infirmary, Glasgow, Scotland); Mezzano S (MD, Departamento de Nefrología, Escuela de Medicina, Universidad Austral, Valdivia, Chile); Schena F (MD, Renal, Dialysis and Transplant Unit, Policlinico, Bari, Italy); Tomino Y (MD, Division of Nephrology, Department of Internal Medicine, Juntendo University School of Medicine, Tokyo, Japan); Walker P (MD, Nephropathology Associates, Little Rock, Arkansas);Wang H (MD, Renal Division of Peking University First Hospital, Peking University Institute of Nephrology, Beijing, China (deceased)); Weening J (MD, Erasmus Medical Center, Rotterdam, The Netherlands); and Yoshikawa N (MD, Department of Pediatrics, Wakayama Medical University, Wakayama City, Japan); the International investigators: Cai-Hong Zeng (MD, Nanjing University School of Medicine, Nanjing, China); Sufang Shi (MD, Peking University Institute of Nephrology, Beijing, China); C.Nogi (MD, Juntendo University, Faculty of Medicine, Tokyo, Japan); H.Suzuki (MD, Juntendo University, Faculty of Medicine, Tokyo, Japan); K. Koike (MD, Division of Nephrology and Hypertension, Department of Internal Medicine, Jikei University School of Medicine, Tokyo, Japan); K. Hirano (MD, Division of Nephrology and Hypertension,

Department of Internal Medicine, Jikei University School of Medicine, Tokyo, Japan); T. Kawamura (MD, Division of Nephrology and Hypertension, Department of Internal Medicine, Jikei University School of Medicine, Tokyo, Japan); T. Yokoo (MD, Division of Nephrology and Hypertension, Department of Internal Medicine, Jikei UniversitySchool of Medicine, Tokyo, Japan); M. Hanai (MD, Division of Nephrology, Department of Medicine, Kurume University School of Medicine, Fukuoka, Japan); K. Fukami (MD, Division of Nephrology, Department of Medicine, Kurume University School of Medicine, Fukuoka,, Japan); K. Takahashi (MD, Department of Nephrology, Fujita Health University School of Medicne, Aichi, Japan); Y. Yuzawa (MD, Department of Nephrology, Fujita Health University School of Medicine, Aichi, Japan); M. Niwa (MD, Department of Nephrology, Nagoya University Graduate School of Medicine, Aichi, Japan); Y. Yasuda (MD, Department of Nephrology, Nagoya University Graduate School of Medicine, Aichi, Japan); S. Maruyama (MD, Department of Nephrology, Nagoya University Graduate School of Medicine, Aichi, Japan); D. Ichikawa (MD, Division of Nephrology and Hypertension, Department of Internal Medicine, St Marianna University School of Medicine, Kanagawa, Japan); T. Suzuki (MD, Division of Nephrology and Hypertension, Department of Internal Medicine, St Marianna University School of Medicine, Kanagawa, Japan); S. Shirai (MD, Division of Nephrology and Hypertension, Department of Internal Medicine, St Marianna University School of Medicine, Kanagawa, Japan); A. Fukuda (MD, First Department of Internal Medicine, Faculty of Medicine, University of Miyazaki, Miyazaki, Japan); S. Fujimoto (MD, Department of Hemovascular Medicine and Artificial Organs, Faculty of Medicine, University of Miyazaki, Miyazaki, Japan); H. Trimarchi (MD, Division of Nephrology, Hospital Britanico, Buenos Aires, Argentina).

Acknowledgement

We thank the International IgA Nephropathy Network for access to the VALIGA data. The authors also thank the NIH Human BioMolecular Atlas Program (HuBMAP) and the Kidney Precision Medicine Project (KPMP) for providing freely available clinical and histology slide data upon which parts of the results in this study are based. The support for manual annotations from Felicitas Weiß is gratefully acknowledged.

Competing Interest Statement

This study was supported by the Immunopathology Working Group of the ERA, the START-Program of the Faculty of Medicine of the RWTH Aachen University (Grant No 148/21), the German Research Foundation (DFG, Project IDs 322900939, 454024652, 432698239 & 445703531), European Research Council (ERC Consolidator Grant No 101001791), and the Federal Ministries of Education and Research (BMBF, STOP-FSGS-01GM1901A), Health (Deep Liver, No. ZMVI1-2520DAT111) and Economic Affairs and Energy (EMPAIA, No. 01MK2002A).

References:

1. Roufosse, C. *et al.* A 2018 Reference Guide to the Banff Classification of Renal Allograft Pathology. *Transplantation* **102**, 1795–1814 (2018).
2. Working Group of the International IgA Nephropathy Network and the Renal Pathology Society *et al.* The Oxford classification of IgA nephropathy: rationale, clinicopathological correlations, and classification. *Kidney Int.* **76**,

936 534–545 (2009).
937 3. Trimarchi, H. *et al.* Oxford Classification of IgA nephropathy 2016: an update
938 from the IgA Nephropathy Classification Working Group. *Kidney Int.* **91**, 1014–
939 1021 (2017).
940 4. Bellur, S. S. *et al.* Reproducibility of the Oxford classification of
941 immunoglobulin A nephropathy, impact of biopsy scoring on treatment
942 allocation and clinical relevance of disagreements: evidence from the
943 VALidation of IGA study cohort. *Nephrol. Dial. Transplant* **34**, 1681–1690 (2019).
944 5. Wilhelmus, S. *et al.* Interobserver agreement on histopathological lesions in
945 class III or IV lupus nephritis. *Clin. J. Am. Soc. Nephrol.* **10**, 47–53 (2015).
946 6. Boor, P. Artificial intelligence in nephropathology. *Nature reviews. Nephrology*
947 vol. 16 4–6 (2020).
948 7. Barisoni, L., Lafata, K. J., Hewitt, S. M., Madabhushi, A. & Balis, U. G. J. Digital
949 pathology and computational image analysis in nephropathology. *Nat. Rev.*
950 *Nephrol.* **16**, 669–685 (2020).
951 8. Bulten, W. *et al.* Automated deep-learning system for Gleason grading of
952 prostate cancer using biopsies: a diagnostic study. *Lancet Oncol.* **21**, 233–241
953 (2020).
954 9. Kanavati, F. *et al.* A deep learning model for the classification of indeterminate
955 lung carcinoma in biopsy whole slide images. *Sci. Rep.* **11**, 8110 (2021).
956 10. Kather, J. N. *et al.* Pan-cancer image-based detection of clinically actionable
957 genetic alterations. *Nat Cancer* **1**, 789–799 (2020).
958 11. Wang, F., Kaushal, R. & Khullar, D. Should Health Care Demand Interpretable
959 Artificial Intelligence or Accept 'Black Box' Medicine? *Ann. Intern. Med.* **172**, 59–

60 (2020).

12. Basu, S., Kolouri, S. & Rohde, G. K. Detecting and visualizing cell phenotype differences from microscopy images using transport-based morphometry. *Proc. Natl. Acad. Sci. U. S. A.* **111**, 3448–3453 (2014).
13. Ilić, S., Stojiljković, N., Sokolović, D., Jovanović, I. & Stojanović, N. Morphometric analysis of structural renal alterations and beneficial effects of aminoguanidine in acute kidney injury induced by cisplatin in rats. *Can. J. Physiol. Pharmacol.* **98**, 117–123 (2020).
14. Rawat, R. R., Ruderman, D., Macklin, P., Rimm, D. L. & Agus, D. B. Correlating nuclear morphometric patterns with estrogen receptor status in breast cancer pathologic specimens. *NPJ Breast Cancer* **4**, 32 (2018).
15. Ruffinatti, F. A., Genova, T., Mussano, F. & Munaron, L. MORPHEUS: An automated tool for unbiased and reproducible cell morphometry. *J. Cell. Physiol.* **235**, 10110–10115 (2020).
16. Zimmermann, M. *et al.* Deep learning-based molecular morphometrics for kidney biopsies. *JCI Insight* **6**, (2021).
17. Bouteldja, N. *et al.* Deep Learning-Based Segmentation and Quantification in Experimental Kidney Histopathology. *J. Am. Soc. Nephrol.* **32**, 52–68 (2021).
18. Helal, I., Fick-Brosnahan, G. M., Reed-Gitomer, B. & Schrier, R. W. Glomerular hyperfiltration: definitions, mechanisms and clinical implications. *Nat. Rev. Nephrol.* **8**, 293–300 (2012).
19. Bülow, R. D., Dimitrov, D., Boor, P. & Saez-Rodriguez, J. How will artificial intelligence and bioinformatics change our understanding of IgA Nephropathy in the next decade? *Semin. Immunopathol.* **43**, 739–752 (2021).

20. Chung, H. *et al.* Joint single-cell measurements of nuclear proteins and RNA in vivo. *Nat. Methods* **18**, 1204–1212 (2021).
21. Ståhl, P. L. *et al.* Visualization and analysis of gene expression in tissue sections by spatial transcriptomics. *Science* **353**, 78–82 (2016).
22. Eng, C.-H. L. *et al.* Transcriptome-scale super-resolved imaging in tissues by RNA seqFISH. *Nature* **568**, 235–239 (2019).
23. Fogo, A. *et al.* Glomerular hypertrophy in minimal change disease predicts subsequent progression to focal glomerular sclerosis. *Kidney Int.* **38**, 115–123 (1990).
24. Coppo, R. *et al.* Validation of the Oxford classification of IgA nephropathy in cohorts with different presentations and treatments. *Kidney Int.* **86**, 828–836 (2014).
25. Hermsen, M. *et al.* Deep Learning-Based Histopathologic Assessment of Kidney Tissue. *J. Am. Soc. Nephrol.* **30**, 1968–1979 (2019).
26. Kleppe, A. *et al.* Chromatin organisation and cancer prognosis: a pan-cancer study. *Lancet Oncol.* **19**, 356–369 (2018).
27. Taylor-Weiner, A. *et al.* A Machine Learning Approach Enables Quantitative Measurement of Liver Histology and Disease Monitoring in NASH. *Hepatology* **74**, 133–147 (2021).
28. Yi, Z. *et al.* Deep learning identified pathological abnormalities predictive of graft loss in kidney transplant biopsies. *Kidney Int.* **101**, 288–298 (2022).
29. Rajpurkar, P., Chen, E., Banerjee, O. & Topol, E. J. AI in health and medicine. *Nat. Med.* **28**, 31–38 (2022).
30. Lu, M. Y. *et al.* AI-based pathology predicts origins for cancers of unknown

primary. *Nature* (2021) doi:10.1038/s41586-021-03512-4.

31. Kers, J. *et al.* Deep learning-based classification of kidney transplant pathology: a retrospective, multicentre, proof-of-concept study. *Lancet Digit Health* **4**, e18–e26 (2022).
32. de Boer, I. H. *et al.* Rationale and design of the Kidney Precision Medicine Project. *Kidney Int.* **99**, 498–510 (2021).
33. HuBMAP Consortium. The human body at cellular resolution: the NIH Human Biomolecular Atlas Program. *Nature* **574**, 187–192 (2019).
34. Isensee, F., Jaeger, P. F., Kohl, S. A. A., Petersen, J. & Maier-Hein, K. H. nnU-Net: a self-configuring method for deep learning-based biomedical image segmentation. *Nat. Methods* **18**, 203–211 (2021).
35. Hao, Y. *et al.* Integrated analysis of multimodal single-cell data. *Cell* **184**, 3573–3587.e29 (2021).
36. Hsu, L. L. & Culhane, A. C. corral: Single-cell RNA-seq dimension reduction, batch integration, and visualization with correspondence analysis. doi:10.1101/2021.11.24.469874.
37. Angerer, P. *et al.* destiny – diffusion maps for large-scale single-cell data in R. doi:10.1101/023309.
38. Granja, J. M. *et al.* ArchR is a scalable software package for integrative single-cell chromatin accessibility analysis. *Nature Genetics* vol. 53 403–411 (2021).
39. Scholz, F. W. & Stephens, M. A. K-Sample Anderson-Darling Tests. *J. Am. Stat. Assoc.* **82**, 918–924 (1987).

Figures & Table

Table 1. Performance metrics for the tissue segmentation convolutional neural network (CNN) and structure segmentation CNN. Segmentation performance of the tissue segmentation CNN was evaluated by calculating Dice-similarity-coefficients (DSCs). Segmentation performance of the structure segmentation CNN was evaluated by averaging all calculated metrics from each instance in all test/external validation images.
iDSC: instance Dice-similarity-coefficient measuring the maximum overlapping area in pixels for each instance between model prediction and ground truth; F1: F1-Score; PPV: Positive predictive value.

Tissue Segmentation CNN												
	AC_B			**AC_N**			**KPMP**			**HuBMAP**		
Class	DSC											
Kidney Tissue	0.99			0.98			0.92			0.99		
Structure Segmentation CNN												
	AC_B			**AC_N**			**KPMP**			**HuBMAP**		
Class	iDSC	F1	PPV	iDSC	F1	PPV	iDSC	F1	PPV	iDSC	F1	PPV
Tubule	0.89	0.93	0.94	0.87	0.92	0.91	0.91	0.94	0.95	0.89	0.94	0.95
Glomerulus	0.93	0.97	0.99	0.91	0.92	0.95	0.94	0.97	0.98	0.92	0.95	0.94
Glomerular Tuft	0.87	0.91	0.90	0.91	0.95	0.95	0.94	0.98	0.98	0.94	0.98	0.99
Non-Tissue Background	0.94	0.96	0.96	0.80	0.84	0.80	0.93	0.96	0.97	0.90	0.92	0.93
Artery	0.73	0.77	0.84	0.64	0.69	0.77	0.64	0.66	0.69	0.70	0.70	0.78
Arterial Lumen	0.72	0.78	0.87	0.52	0.56	0.59	0.59	0.63	0.75	0.71	0.78	0.86

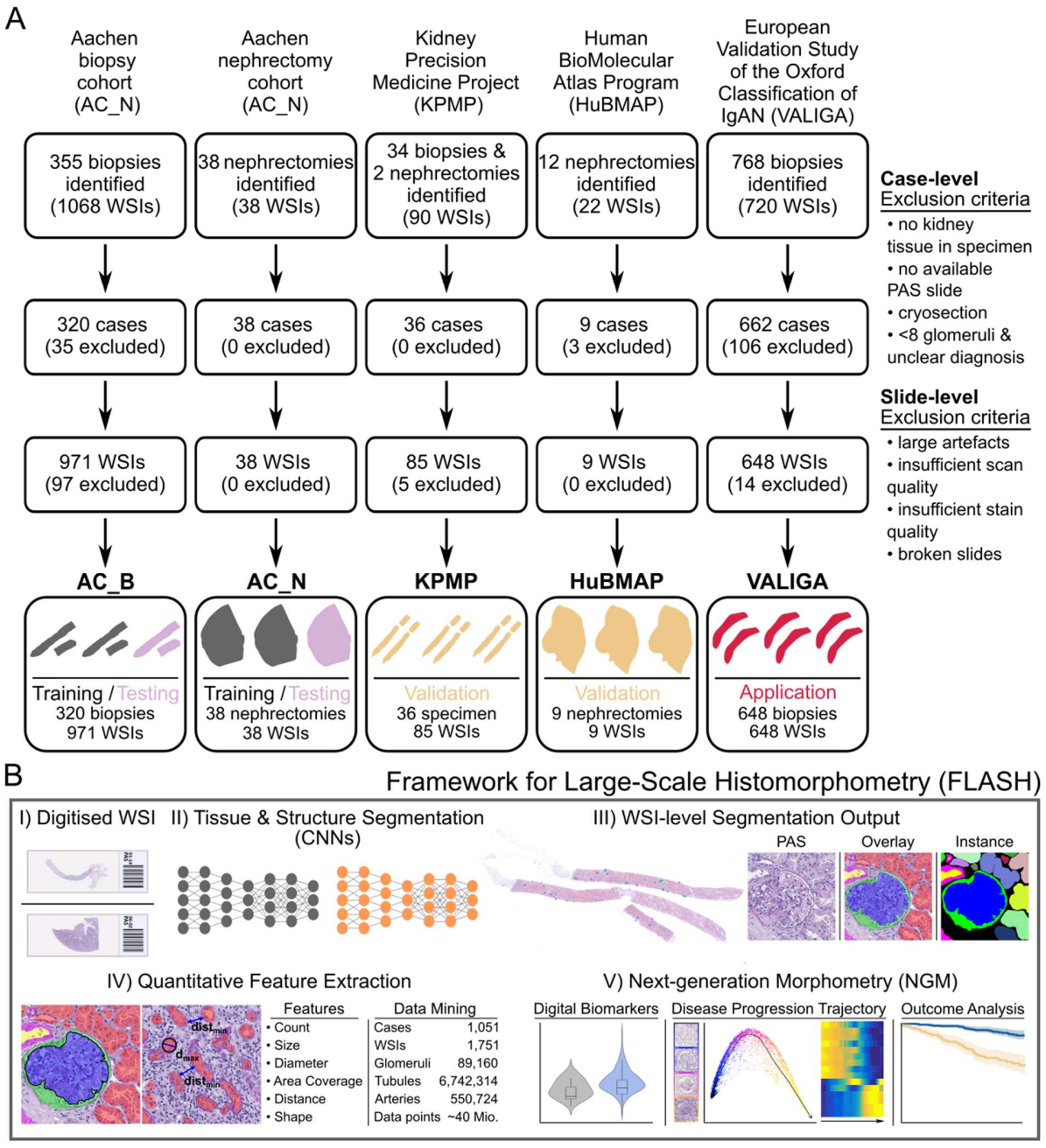

Figure 1. Flowchart of the patient cohorts and the integration of our framework for large-scale histomorphometry (FLASH) into a digital pathology workflow. (A) Overview of the cohort refinement process. Cases and whole-slide images (WSIs) were excluded based on predefined criteria on case- and slide-level. 1,051 cases from five cohorts and 1,751 WSIs were included in this study. (B) Integration of FLASH into the digital pathology workspace. FLASH combines deep learning-based segmentation with bioinformatics analysis of quantitative morphometric features. The framework consists of two convolutional neural networks (CNNs) for tissue and structure segmentation, computational feature extraction and Next-generation Morphometry (NGM) analysis.
IgAN: IgA nephropathy; WSIs: Whole-slide images; PAS: Periodic Acid Schiff.

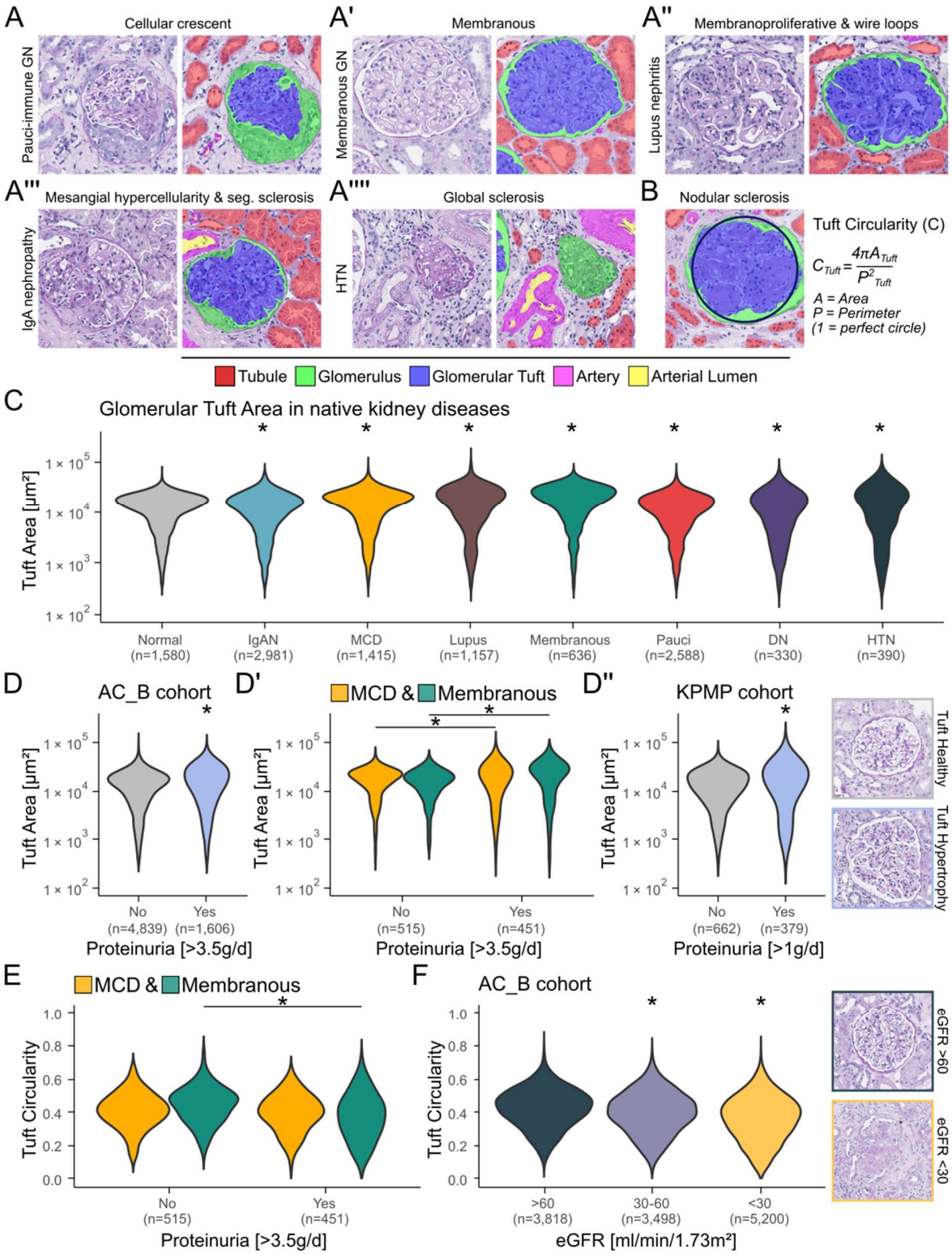
A
Cellular crescent
Pauci-immune GN
A'
Membranous
Membranous GN
A''
Membranoproliferative & wire loops
Lupus nephritis
A'''
Mesangial hypercellularity & seg. sclerosis
IgA nephropathy
A''''
Global sclerosis
HTN
B
Nodular sclerosis
Tuft Circularity (C)
$C_{Tuft} = \frac{4\pi A_{Tuft}}{P^2_{Tuft}}$
A = Area
P = Perimeter
(1 = perfect circle)
Tubule
Glomerulus
Glomerular Tuft
Artery
Arterial Lumen
C
Glomerular Tuft Area in native kidney diseases
Tuft Area [µm²]
Normal (n=1,580)
IgAN (n=2,981)
MCD (n=1,415)
Lupus (n=1,157)
Membranous (n=636)
Pauci (n=2,588)
DN (n=330)
HTN (n=390)
D
AC_B cohort
D'
MCD & Membranous
D''
KPMP cohort
No (n=4,839)
Yes (n=1,606)
Proteinuria [>3.5g/d]
No (n=515)
Yes (n=451)
Proteinuria [>3.5g/d]
No (n=662)
Yes (n=379)
Proteinuria [>1g/d]
Tuft Healthy
Tuft Hypertrophy
E
MCD & Membranous
Tuft Circularity
No (n=515)
Yes (n=451)
Proteinuria [>3.5g/d]
F
AC_B cohort
>60 (n=3,818)
30-60 (n=3,498)
<30 (n=5,200)
eGFR [ml/min/1.73m²]
eGFR >60
eGFR <30

Figure 2: NGM-derived glomerular features reveal distinct morphometric patterns in native kidney diseases and different clinical conditions, such as nephrotic range proteinuria and reduced kidney function. (A-A"") Segmentation visualisations of glomeruli in major glomerular injury patterns (images stem from the internal *AC_B* cohort excluding training samples). (B) Visual representation for calculation of glomerular tuft circularity as an example of one of the extracted morphometric features. (C) Comparison of glomerular tuft area [μm^2] with 11,077 instances in different native kidney diseases from the *AC_B* cohort. Glomeruli from biopsies without pathological findings were used as a control (depicted in grey). (D) Feature analysis of glomerular tuft area based on nephrotic range proteinuria in all native biopsies from the *AC_B* cohort, (D') for glomeruli from biopsies diagnosed with minimal change disease (MCD) or membranous glomerulonephritis (GN) and (D") for glomeruli with large proteinuria from the external *KPMP* cohort. Visualisations highlight the increase in glomerular tuft area in cases with nephrotic range proteinuria. (E) Comparison of glomerular tuft circularity between cases of MCD and membranous GN with or without nephrotic range proteinuria. (F) Analysis of glomerular tuft shape based on reported estimated glomerular filtration rate in all native biopsies from our internal biopsy cohort including additional visualisation examples. All displayed patches of histopathology images have an edge length of 300μm.
GN: Glomerulonephritis; Seg.: Segmental; HTN: Hypertensive nephropathy; IgAN: IgA nephropathy; MCD: Minimal change disease; Membranous: Membranous glomerulonephritis; Pauci: Pauci-immune glomerulonephritis, DN: Diabetic nephropathy; eGFR: estimated glomerular filtration rate. * = $p < 0.05$.

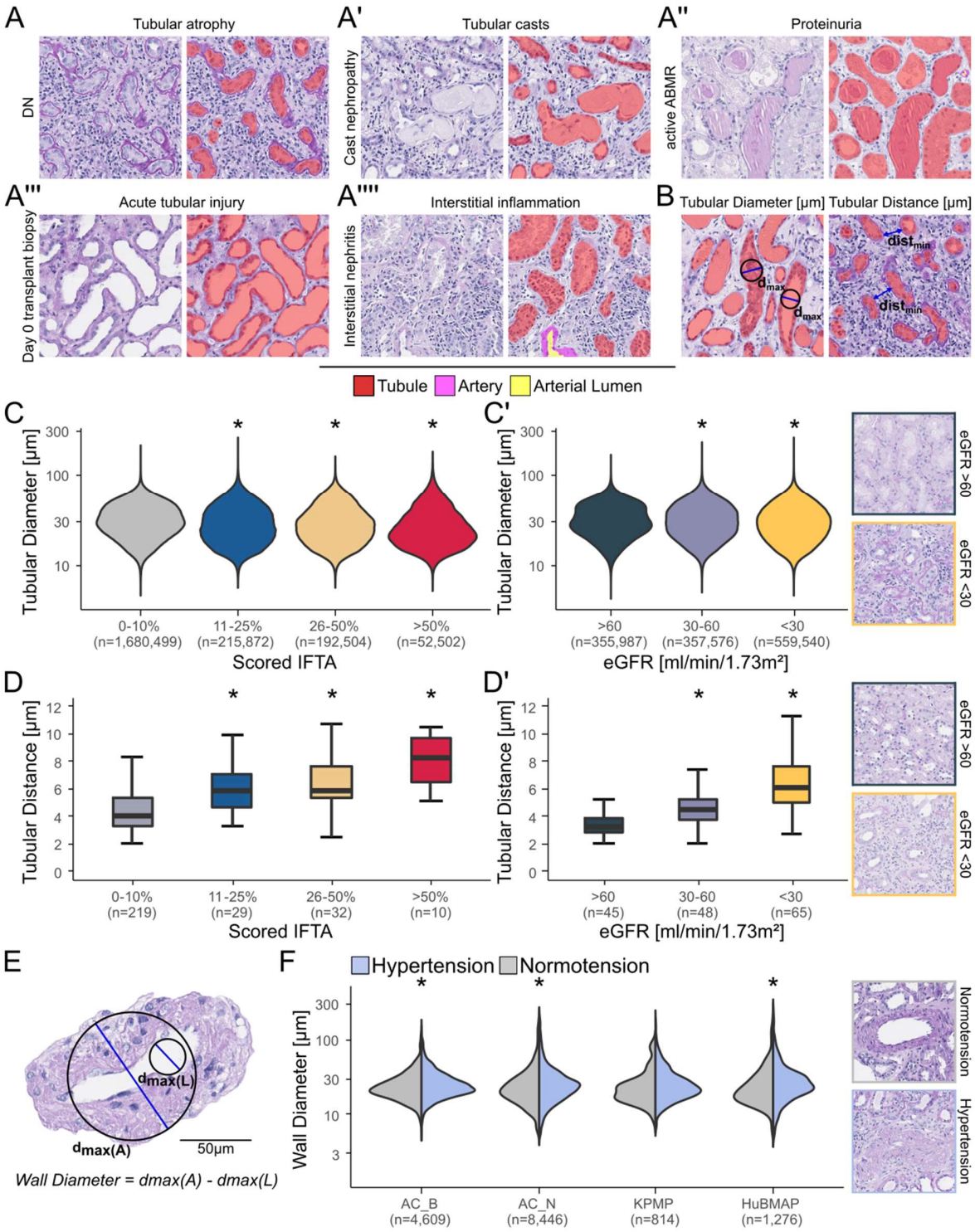
A
Tubular atrophy
DN
A'
Tubular casts
Cast nephropathy
A''
Proteinuria
active ABMR
A'''
Acute tubular injury
Day 0 transplant biopsy
A''''
Interstitial inflammation
Interstitial nephritis
B
Tubular Diameter [µm]
Tubular Distance [µm]
Tubule
Artery
Arterial Lumen
C
Tubular Diameter [µm]
0-10% (n=1,680,499)
11-25% (n=215,872)
26-50% (n=192,504)
>50% (n=52,502)
Scored IFTA
C'
>60 (n=355,987)
30-60 (n=357,576)
<30 (n=559,540)
eGFR [ml/min/1.73m²]
eGFR >60
eGFR <30
D
Tubular Distance [µm]
0-10% (n=219)
11-25% (n=29)
26-50% (n=32)
>50% (n=10)
Scored IFTA
D'
>60 (n=45)
30-60 (n=48)
<30 (n=65)
eGFR [ml/min/1.73m²]
E
dmax(L)
dmax(A)
50µm
Wall Diameter = dmax(A) - dmax(L)
F
Hypertension
Normotension
Wall Diameter [µm]
AC_B (n=4,609)
AC_N (n=8,446)
KPMP (n=814)
HuBMAP (n=1,276)
Normotension
Hypertension

Figure 3: NGM-derived features of tubules and arteries are associated with pathologist derived scoring and clinical hypertension status. (A-A"") Segmentation visualisations of tubules with large variation in size and shape in various diseases and morphological injury patterns present in the patch. Visualisations stem from the internal *AC_B* cohort excluding training samples. (B) Visual representation of feature calculation of tubular diameter and tubular distance. (C) Feature analysis of tubular diameter based on the quantified amount of interstitial fibrosis and tubular atrophy (IFTA) of all biopsies with reported IFTA from the *AC_B* cohort. (C') Analysis of tubular diameter based on the measured estimated glomerular filtration rate (eGFR) of all native biopsies from our internal biopsy cohort. (D) Feature analysis of tubular distance based on the quantified IFTA of all biopsies with reported IFTA from the internal biopsy cohort. (D') Analysis of tubular distance based on the measured eGFR of all native biopsies from our internal biopsy cohort. (E) Feature visualisation for arterial/arteriolar wall diameter. (F) Analysis of the wall diameter based on the presence of hypertension regardless of aetiology in two internal and two external cohorts where hypertension status was reported. All displayed patches of histopathology have an edge length of 300µm.
DN: Diabetic nephropathy; ABMR: Antibody-mediated rejection; d: Instance diameter; IFTA: Interstitial fibrosis and tubular atrophy; eGFR: estimated glomerular filtration rate. * = $p < 0.05$.

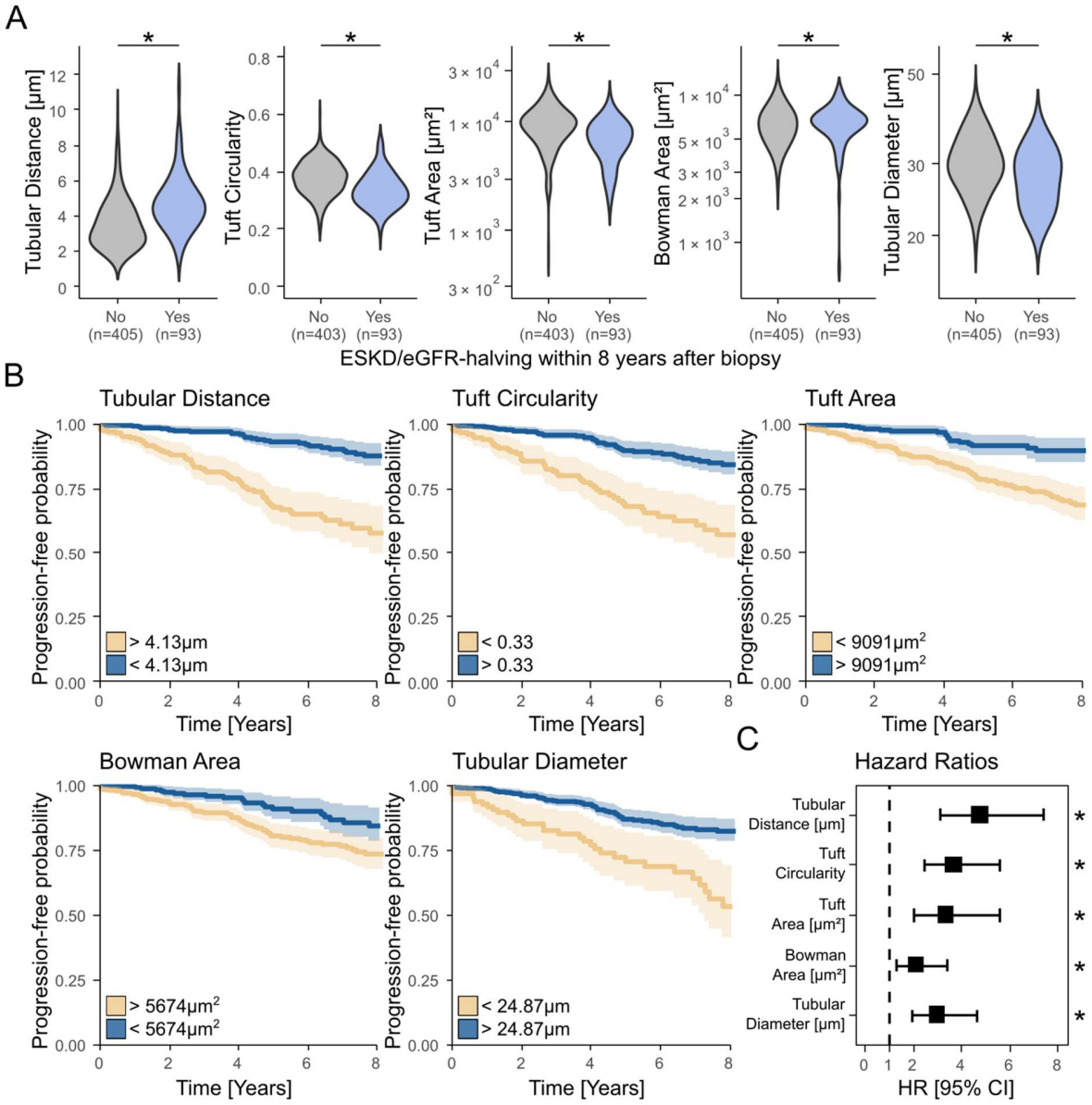

Figure 4: NGM-derived quantitative features are predictive of disease progression in IgA nephropathy (IgAN). (A) Comparison of five predictive digital biomarkers based on reaching the defined combined endpoint, i.e., end-stage kidney disease and/or halving of initial estimated glomerular filtration rate (eGFR) within 8 years after biopsy. (B) Univariate Cox regression models for the five predictive features summarised at patient-level including the hazard ratios of each individual feature. Cumulative events for each group in the univariate Cox regression models are provided in Supp. Table 10. (C) Hazard ratios and their 95% confidence interval from the univariate Cox regression models of the respective features.

ESKD: End-stage kidney disease; eGFR: estimated glomerular filtration rate; HR: Hazard ratio; CI: Confidence interval. * = $p < 0.05$.

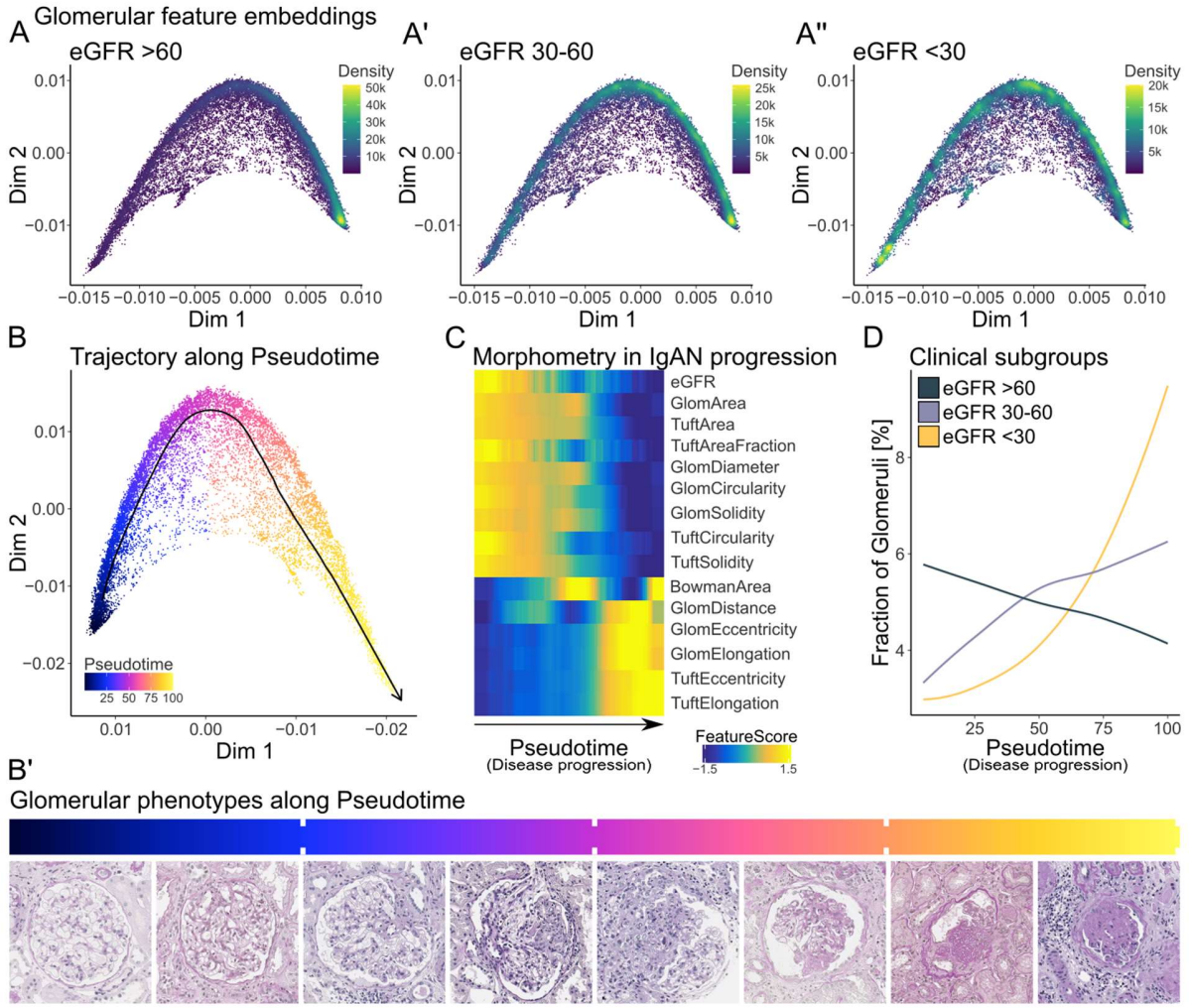

Figure 5: Pseudotime analysis of NGM-derived glomerular features identifies distinct glomerular groups along a trajectory of disease progression in IgA nephropathy (IgAN). (A-A") Diffusion map embedding of 24,227 glomerular instances with 14 morphometric features with IgAN based on the reported estimated glomerular filtration rate (eGFR) [ml/min/1.73m²]. (B) Diffusion mapping of glomerular instances with pseudotime indicating ordering of glomerular instances along their progression from healthy to diseased. (B') Visualisation of glomerular phenotypes along the pseudotime. (C) Scaled feature expression heatmap including eGFR along the pseudotime trajectory. (D) Morphometric progression of glomerular instances in clinical subgroups based on the overall reported eGFR.

eGFR: estimated glomerular filtration rate; Dim: Diffusion map; IgAN: IgA nephropathy.

Supplementary Files

This is a list of supplementary files associated with this preprint. Click to download.

- NGMSuppl.pdf